Nanoscopic Characteristics of Anhydrite (100) Growth

Juan Morales,[†] José Manuel Astilleros,[†,‡] and Lurdes Fernández-Díaz*[,†,‡]

[†] Departamento de Cristalografía y Mineralogía, Universidad Complutense de Madrid, 28040 Madrid, Spain

[‡] Instituto de Geociencias (UCM-CSIC), C/José Antonio Novais 2, 28040 Madrid, Spain

ABSTRACT: The growth of anhydrite (100) surface in contact with supersaturated aqueous solutions ($\beta_{anh} = 1 - 3.6$) under low hydrothermal conditions ($T = 60 - 120$ °C) has been studied by use of a hydrothermal atomic force microscope (HAFM). Our observations show that growth on this surface occurs by lateral spreading of monomolecular layers (3.5 Å in height) and is highly anisotropic, with [001] and [001] alternating as fast and slow directions in successive monolayers. This anisotropic growth is evidence of strong structural control, which becomes less intense as temperature and/or supersaturation increases. The growth anisotropy affects the development of spirals, determining the combination of fast-moving and slow-moving steps to form bilayer steps around the emergence point of screw dislocations and leading to nonconstant spread rates.

As a result, the overall efficiency of spiral growth mechanism is highly dependent on the interaction between slow-moving bilayers and fast-moving monolayers originating from different dislocations.

Formation of two-dimensional nuclei occurs only at $T \geq 80$ °C and $\beta_{anh} \geq 2$, two-dimensional nucleation density always being very low (≤ 1 nucleus/μm^2) under the conditions explored. These facts, together with the slow kinetics of anhydrite growth in comparison to the much faster kinetics of gypsum growth, might explain the frequent metastable formation of gypsum crystals under temperatures corresponding to the stability field of anhydrite.

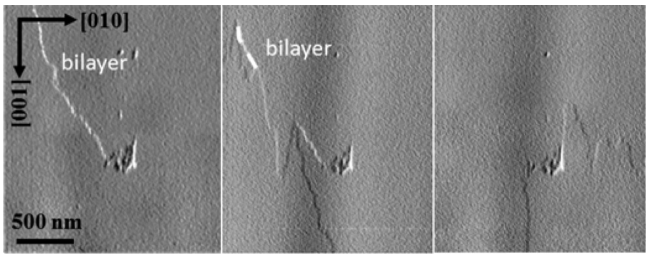

INTRODUCTION

Gypsum ($CaSO_4 \cdot 2H_2O$), hemihydrate ($CaSO_4 \cdot 0.5H_2O$), and anhydrite ($CaSO_4$) are the only calcium sulfate phases that can be found in natural environments. Gypsum is the most abundant sulfate mineral and a major component of evaporites. Hemihydrate is less common and its formation is limited to very specific natural environments.[1] Anhydrite, though less abundant than gypsum, is also a major component of evaporites in both sediments and some hydrothermal systems. The origin of sedimentary anhydrite is diverse, and evidence supporting a primary origin and a secondary origin after gypsum has been reported. The transformations between $CaSO_4$ minerals occurring in the so-called "gypsum−anhydrite cycle" play a key role in the genesis and evolution of evaporites.[2] Recently, an anhydrite dissolution− gypsum crystallization process has been considered to be in the origin of the formation of giant gypsum crystals, for example in the Naica (Chihuahua, Mexico) setting.[3,4] Moreover, anhydrite is a widespread mineral in modern submarine hydrothermal fields, where it precipitates from mixing of hydrothermal fluids and seawater.[5] It is well documented that cycles of anhydrite dissolution/precipitation affect the permeability of hydrother-mal structures, thereby influencing the circulation of fluids[6,7] and the distribution of trace elements (Sr, Y, REE) within hydrothermal deposits.[8] Therefore, anhydrite formation is significant to the geochemical cycling of sulfur, calcium, and a number of trace elements.

In addition, CaSO4 has important industrial applications, especially in the building and constructioni ndustries and in the manufacturing of glasses, fertilizers, phar-maceutical products, etc.[9] On the other hand, $CaSO_4$ minerals often appear as components of undesirable scale in industrial processes like water and wastewater treatment, gas/oil produc-tion, etc.[10,11] The deposition of $CaSO_4$ scale reduces heat transfer coefficient and, consequently, the thermal efficiency of technological processes. $CaSO_4$ scale mainly consists of gypsum, but both hemihydrate and anhydrite also often occur.[12] Anhy-drite scale most commonly forms on hot metal surfaces, with gypsum forming on top of the anhydrite.[13] Different researchers that have studied the crystallization of $CaSO_4$ phases, at condi-tions similar to those occurring in a range of technological processes, found it striking that anhydrite failed to form from solutions markedly supersaturated with respect to this phase at any temperature.[11,13]

While the characteristics of gypsum dissolution and growth are fairly well-known at both macro and molecular scale,[4,14−18] much less attention has been paid to the formation of either hemihydrate or anhydrite. Although the gypsum−anhydrite equilibrium temperature in water is controversial (values ranging from 42 ± 2 °C t o 58 ± 2 °C[19,20] have been reported), there is general agreement that anhydrite is metastable under room-temperature conditions. In spite of this, all previous attempts to

study the molecular mechanisms of anhydrite dissolution and growth have been conducted at 25 °C and 1 atm.[21−29]

Anhydrite crystallizes in the orthorhombic system, space group *Amma*, with lattice parameters a_0 = 6.993 Å, b_0 = 6.995 Å, and c_0 = 6.245 Å. Its structure can be regarded as chains of alternating edge-sharing SO_4 tetrahedra and CaO_8 dodecahedra that extend along [001]. These chains are linked along [100] by edge-sharing of the CaO_8 dodecahedra and corner-sharing SO_4 tetrahedra and along [010] by corner-sharing between SO_4 tetrahedra and CaO_8 dodecahedra.[30,31] This structure allows perfect to good cleavage parallel to (010), (100), and (001). Atomistic simulations confirmed these surfaces as the most stable ones and showed that on relaxation they are bulk-terminated.[32] These surfaces can be classified as F-faces, according to the Hartman−Perdock model.[27,33−35]

In this work, we apply hydrothermal atomic force microscopy (HAFM) to study the growth of anhydrite (100) surfaces in contact with aqueous solutions at different saturation states at temperatures of 60−120 °C and pressure of 1 bar. We focus on (100) surface because, together with (010) surfaces, these are the most important ones for the morphology of natural anhydrite crystals. Our aim is to study the molecular mechanisms that control the growth of this surface under conditions within the stability field of anhydrite. Understanding the nanoscale characteristics of growth of anhydrite surface will allow us to draw general conclusions regarding crystallization in the $CaSO_4$−H_2O system.

EXPERIMENTAL METHODS

Experiments on anhydrite (100) surface were conducted at the Department of Geo- and Environmental Sciences of the Ludwig-Maximilians University of Munich (Germany), on a self-constructed hydrothermal atomic force microscope (HAFM).[35,36] This device allows in situ investigations of processes that occur at the solid−liquid interface at temperatures up to 170 °C and pressures up to 50 bar. The atomic force microscope was operated in contact mode, using constant force mode and uncoated Si cantilevers with integrated tips (spring constant = 0.2 N/m). All experiments were performed on natural slightly blue anhydrite crystals from Naica, Chihuahua (Mexico). X-ray fluorescence spectroscopic analysis of these crystals revealed that they contained less than 0.4 wt % impurities, with Sr as the main impurity. Prior to the experiments, the crystals were first oriented with respect to their main crystallographic directions, which were located by observing the interference figures of different sections by means of a polarized optical microscope. Then the crystals were cleaved with a knife edge parallel to (100). The samples were placed within the HAFM fluid cell and mechanically affixed by a passivated titanium wire. The fluid cell (volume = 500 μL) was then filled with solution, sealed, pressurized to ∼1 bar above ambient with N_2 to prevent the formation of bubbles, and heated. N_2 had no contact with the solution in the fluid reservoirs and the HAFM cell. A continuous gravitationally controlled flow of solution at a constant rate (3−6 μL/s) was ensured by a mass flow controller. The experiments were run at temperatures from 60 to 120 °C. The orientation of the surface was confirmed on the basis of its dissolution features.

The solutions were prepared by adding $CaCl_2$, Na_2SO_4, and NaCl reagent-grade compounds to high-purity deionized water (resistivity = 18.2 MΩ·cm). Specific solution compositions used are listed in the Supporting Information, Table S1. In all cases the $a(Ca^{2+})/a(SO_4^{2-})$ ratio was ∼1.4. An approximately constant ionic strength was assured by adjusting a 15 mM NaCl concentration. Aqueous solution supersaturation was defined by $\beta_{anh} = a(Ca^{2+})a(SO_4^{2-})/K_{anh}$. $\beta_{anh} > 1$ values are supersaturated, and $\beta_{anh} < 1$ values are undersaturated. Calcium and sulfate concentrations were calculated by use of the numerical code PHREEQC (database phreeqc).[37]

Computer models of anhydrite structure were constructed by use of CrystalMaker software.[38]

Figure 1. Anhydrite (100) surface dissolving in water at 120 °C. Steps at pits are oriented parallel to [001] and ⟨011⟩ directions. Most steps consist of several monolayers. White arrows indicate monolayer step (3.5 Å in height). The scan direction was down.

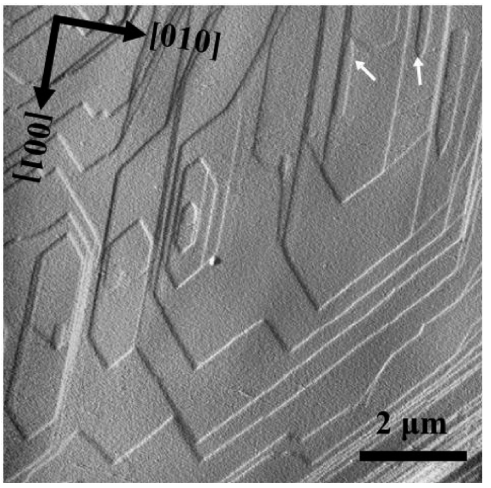

Figure 2. AFM deflection images showing the orientation characteristics of growth steps and dendritelike growth fronts spreading on a (100) anhydrite surface. Growth occurs by lateral spreading of half unit cell (3.5 Å) monolayers. The scan direction was up.

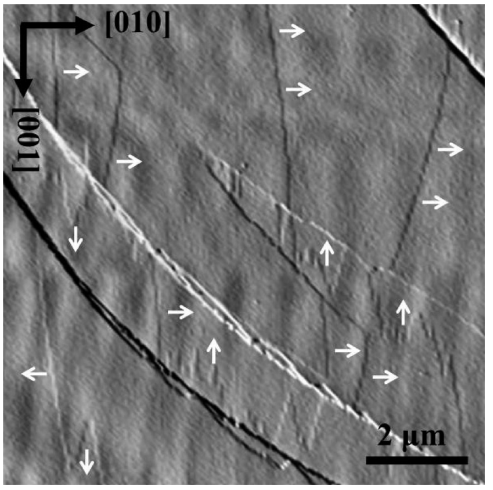

RESULTS

Cleavage Step Growth. Freshly cleaved anhydrite (100) surfaces typically consisted of atomically flat terraces bounded by cleavage steps parallel to [010], [001], and, less frequently, ⟨011⟩ directions. In contact with pure water, shallow pencil-shaped and deep pseudohexagon-shaped etch pits nucleated on this surface (Figure 1). Both types of etch pits rapidly became elongated along [001]. Shallow etch pits were 3.5 Å in depth, which is consistent with a half unit cell in the anhydrite lattice. The orientation of the etch pits enabled defining the main crystallographic directions on anhydrite (100) surface.[24]

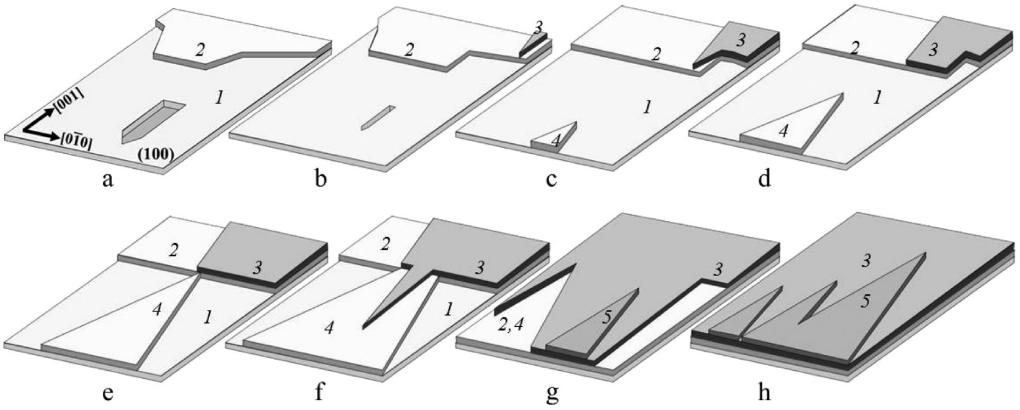

Figure 3. Schematic illustrating the alternation of fast and slow dendritelike growth fronts moving along <001> direction on anhydrite (100) surface.

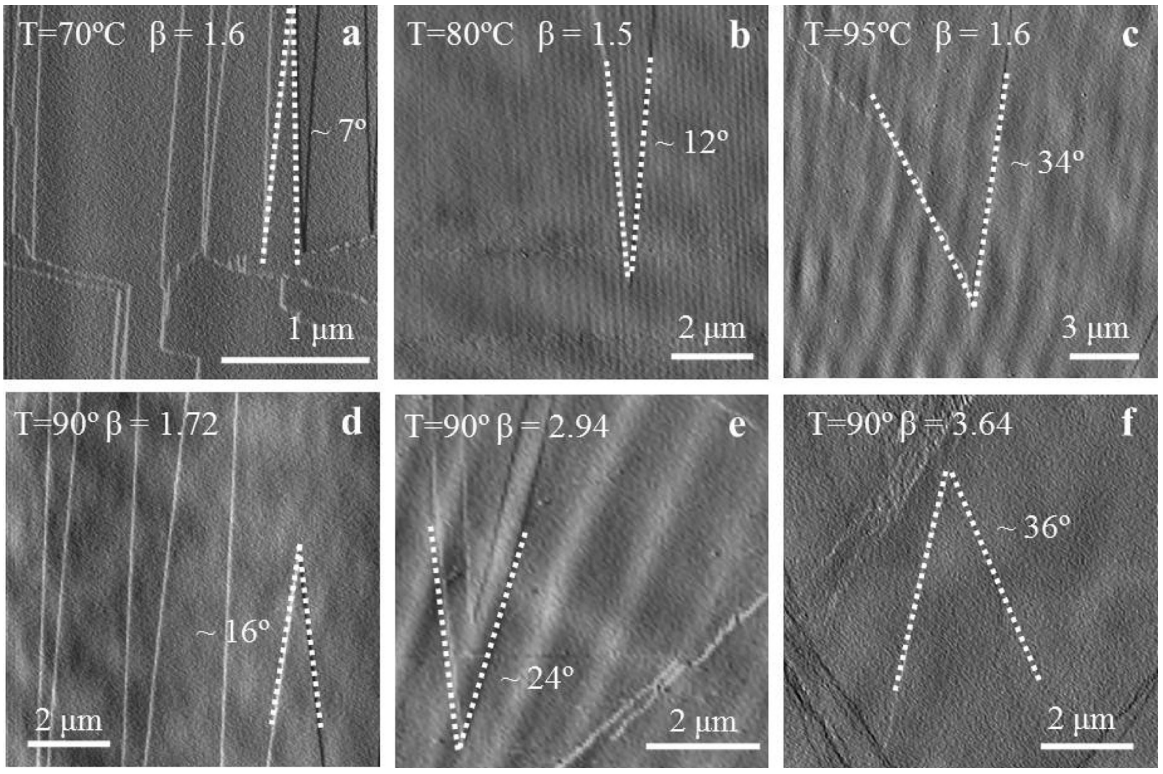

Figure 4. AFM deflection images showing examples of different dendritelike fronts moving along ⟨001⟩. Different shapes (step orientations) can be distinguished as a function of temperature and supersaturation. The scan direction was down in panels a, d, and f and up in panels b, c, and e.

In contact with supersaturated solutions, growth was observed to occur on (100) surface by lateral spreading of monomolecular layers (3.5 Å in height) that originated at the cleavage steps. The advancement of these monomolecular layers was highly anisotropic. Figure 2 illustrates the spreading behavior of the differently oriented steps. Steps parallel to [001] directions remained straight during their lateral spreading and moved at moderate rates (5 ± 1.3 nm/s at $T = 80$ °C and $\beta_{anh} = 1.83$; 40 ± 6 nm/s at $T = 110$ °C and $\beta_{anh} = 2.81$). Steps parallel to [010] were highly unstable and behaved differently in the alternating monolayers. While in one monolayer [010] steps moving along [001] advanced at high speed, becoming strongly jagged and disappearing into dendritelike fronts soon after growth started, [010] steps moving along [00$\bar{1}$] remained straight and showed negligible advancement. The situation was reversed in the subsequent monolayer, where [010] steps advanced rapidly along [00$\bar{1}$] and remained virtually static along [001]. The fast-moving dendritelike fronts advanced at rates of 20 ± 3.2 nm/s at $T = 80$ °C and $\beta_{anh} = 1.83$. Under higher T and β_{anh}, the very fast advancement of these steps made it impossible to measure their spreading rates. Finally, straight steps initially parallel to [011] rapidly became curved, changing their orientation as soon as growth started. This change in orientation was less evident when growth occurred at higher temperatures and supersaturations.

Figure 3 schematizes the anisotropic behavior of growth along ⟨001⟩ directions. In Figure 3b, a fast-moving dendritelike front (denoted as 3) advances along the [00$\bar{1}$] direction to reach the slow-moving [010] step (denoted as 2) of the monolayer

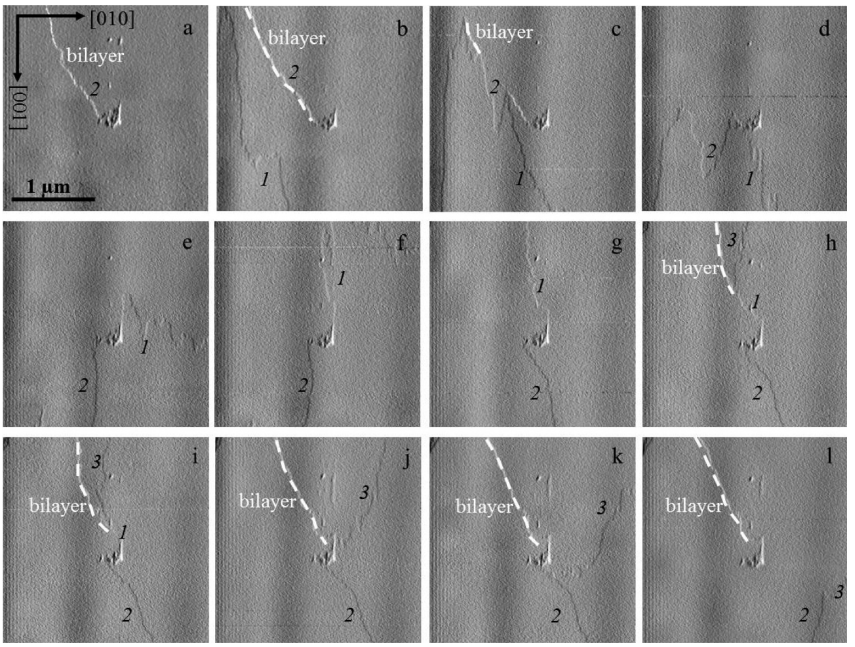

Figure 5. Sequence of AFM deflection images of a spiral on a (100) anhydrite face taken at β_{anh} = 2.12 and T = 90 °C. The sequence illustrates the change in advancement rate as the orientation of the steps changes. Bilayer steps form where a fast-moving step catches up with a slow-moving step (b, c, h–l). Spiral growth is reactivated as a result of interaction with fast-moving steps originating at cleavage steps or other screw dislocations (c, d, k, l). White broken lines indicate the location of bilayer steps.

underneath in Figure 3c,d. At this point a bilayer [010] step forms (Figure 3d–f). This bilayer step remains virtually static until a fast-moving monolayer front (denoted as 4) advancing in the [001] direction reaches it and coalesces with 2 (Figure 3e), providing a surface on which monolayer 3 can spread. At this point, monolayer 3 resumes its growth, fast-moving along [00$\bar{1}$] on monolayer 4 (Figure 3f). Finally, a subsequent monolayer (denoted as 5) spread on monolayer 3, moving fast in the opposite [001] direction and defining a dendritelike growth front.

Growth fronts moving fast along [001] and [00$\bar{1}$] in successive monolayers consisted of dendritelike tips. The dendrites were bounded by steps that defined an acute angle. The orientation of the bounding steps and therefore the sharpness of the dendrite tips varied as a function of both temperature and supersaturation. When growth occurred at low temperatures and/or low supersaturation conditions, the dendrites showed sharp tips and were bounded by rough steps defining angles <10°. Increasing temperatures and/or supersaturations caused the step angles to evolve toward less acute. Whereas at a supersaturation β_{anh} ~ 1.6 the measured angle was 8° ± 2° at 70 °C, it increased to 40° ± 8° at 95 °C. Similarly, at 90 °C we measured angles of 15° ± 5° when the supersaturation was β_{anh} = 1.7 and of 40° ± 6° when the supersaturation was β_{anh} = 3.6. Figure 4 depicts several examples of differently sharp dendrites at different temperatures and supersaturations.

Screw Dislocation Growth. Screw dislocation growth was observed in a number of experiments. Figure 5 shows a typical sequence of spiral growth. It is noteworthy that the high anisotropy of growth observed in the advancement of growth fronts parallel to ⟨001⟩ is clearly reflected by the movement of the steps around the screw dislocation. In Figure 5a, a curved step (denoted 2) with origin in the emergence point of the screw dislocation can be observed. This step consists of two mono-layers. The white broken lines in Figure 5b mark the location of

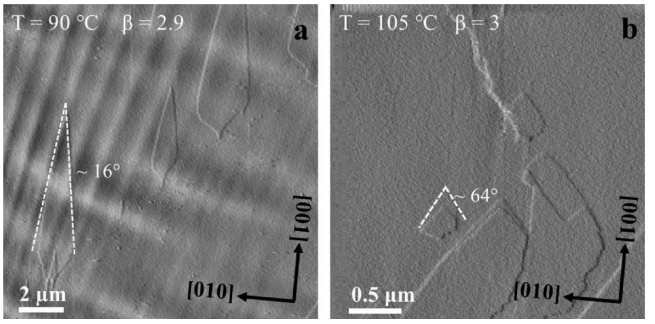

Figure 6. HAFM images showing the effect of temperature and supersaturation on the shape of two-dimensional islands growing on anhydrite (100) surface. The scan direction was down in both images.

bilayer steps along the growth sequence. Step 2 remains virtually immobile (Figure 5b) because the fast-moving direction of its upper monolayer coincides with the slow-moving direction of its lower monolayer. When a half unit cell high growth front (denoted 1), which moves rapidly upward the image, merges with the lower monolayer of step 2 (Figure 5c), its upper monolayer can resume its growth and rapidly advances downward the image as a dendritic front (Figure 5c,d). Growth front 1 continues to advance toward the right and subsequently upward in the image (Figure 5d–f). Images in Figure 5f,g depict how, as growth fronts 1 and 2 turn around the emergence point of the dislocation to advance along their respective slow-moving directions, both become stabilized as steps approximately parallel to ⟨001⟩ and advance at moderate speed along [0$\bar{1}$0] and [010], respectively (Figure 5f,g). As time progresses, a new fast-moving growth front (denoted 3) rapidly advances downward (Figure 5h) to contact growth front 2 in the down-right part of the image in Figure 5k,l. The part of this front that reaches step 1 cannot progress advancing because its

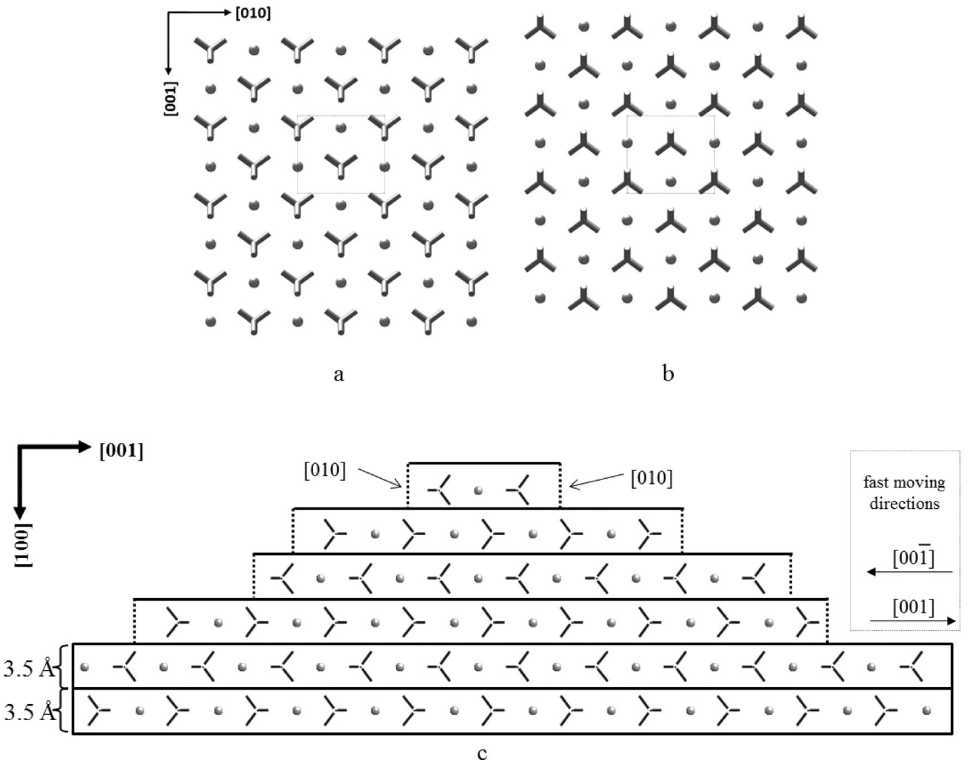

Figure 7. (a) Structure of one anhydrite half unit cell growth monolayer projected along [100] direction. (b) Equivalent projection of the previous and next half unit cell growth monolayers. Both projections are related by a 180° rotation, corresponding to the existence of a 2_1 axis along [100] in anhydrite structure. (c) Projection along [010] showing the opposite orientation of sulfate groups in successive monolayers. The different geometry of parallel [010] steps that advance along [001] and [00$\bar{1}$] within the same monolayer is evidenced.

fast-moving direction coincides with the slow-moving direction of the monolayer underneath. At this point, a new bilayer step forms. This bilayer step (see broken line in Figure 5h–l) reproduces a topography similar to that of growth front 2 in Figure 5a,b.

Two-Dimensional Nucleus Formation. On a few occasions, the formation of two-dimensional nuclei was observed. In all these cases, the supersaturation with respect to anhydrite (β_{anh}) was ≥2 and the temperature was ≥80 °C. The nucleation density always was very low, with a maximum of 1 nucleus/μm^2. Although in most cases two-dimensional nuclei formed on clean areas of the surface, some appeared related to defects or impurities. A clear relationship between nucleation density, supersaturation, and temperature could not be established. Examples of two-dimensional islands growing on a (100) anhydrite surface in contact with a supersaturated solution ($\beta_{anh} \sim 3$) at T = 90 and 105 °C are depicted in Figure 6.

Two-dimensional nuclei, as described above for growth steps, always were a half unit cell in height (3.5 Å) and showed strongly anisotropic growth. Two-dimensional islands mainly grew along ⟨001⟩, while their development along the perpendicular direction [010] was much more limited. Furthermore, growth parallel to ⟨001⟩ also was highly anisotropic, with one end advancing rapidly and the opposite virtually immobile. The rates of advancement of the fast- and slow-moving ends of two-dimensional islands could be measured in several cases. The ratio between the two values measured on islands growing at T = 80 °C from a solution with supersaturation β_{anh} = 2.13 was ~38. This ratio decreased to ~29 in two-dimensional islands growing at T = 95 °C from a solution with supersaturation β_{anh} = 2.53. The marked anisotropic growth determined that two-dimensional islands developed an elongated pseudotriangular morphology, with a sharp pencil-like fast-moving tip and a slow-moving base with a slightly curved growth front. The angle measured in the sharp pencil-like tip varied with temperature and supersaturation. This change showed similar characteristics to that undergone by the angle between steps in the dendritelike growth fronts advancing along ⟨001⟩ directions. Thus, the angle measured between the steps bouncing the fast-moving tip in two-dimensional islands became progressively less acute as supersaturation and/or temperature were increased (compare two-dimensional islands in Figure 6 panels a and b). Due to the low two-dimensional nucleation density, island coalescence was not observed in any of our experiments.

DISCUSSION

Monolayer Spread Characteristics. In the range of temperatures and supersaturations considered in this study, anhydrite growth occurs by a layer-by-layer mechanism, controlled by step advancement along [010] and ⟨001⟩. The general characteristics of monolayers spread are similar to those reported by Shindo et al.[24−27] for the anhydrite (100) dissolution in contact with undersaturated solutions of different composition and by Pina[29] for the growth of this surface from supersaturated solutions, in both cases at 25 °C, which evidence that the strong structural control of both anhydrite (100) dissolution and growth at room temperature extends into higher temperature conditions. This structural control determines a highly anisotropic growth, characterized by very different monolayer spread speeds along [010] and along ⟨001⟩. While straight [001] steps advance along [010]

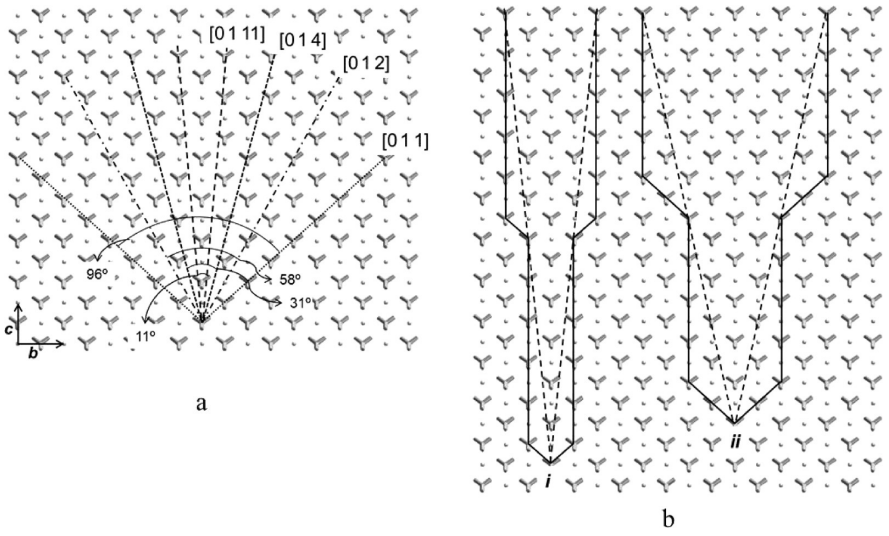

Figure 8. (a) Sketch showing low index directions on the (100) surface of anhydrite. As is apparent from Figures 4 and 6, the angle between steps vicinal to [001] and [011] increases with temperature and supersaturation. Their orientation changes from roughly [0 1 11] (angle ~10°) to [012] (angle ~60°). (b) Structure of straight steps in the sharp tips in two-dimensional islands and fast moving growth fronts. Example I corresponds to lower temperature and supersaturation conditions than example ii.

at slow speeds, growth fronts move very rapidly along ⟨001⟩, with [001] and [00$\bar{1}$] alternating as fast-moving directions in successive monolayers. The ratio between measured fast spread speed along ⟨001⟩ and along [010] ($S_{\langle 001\rangle}/S_{[010]}$) is >5 when growth occurs under low temperature and supersaturation. The large difference in spread speeds can be related to the stability of calcium sulfate chains in anhydrite structure. Calcium sulfate chains parallel to [001] are strongly bonded and straight, and consequently contain a low density of kink sites.[21−27] These characteristics explain the stability of [001] steps and their slow movement along ⟨010⟩. Moreover, the advancement of these steps occurs at the same speed along [010] and [0$\bar{1}$0], in agreement with the mirror plane parallel to (001) that runs parallel to these calcium sulfate chains. On the other hand, the development of fast-moving growth fronts along ⟨010⟩ is consistent with the fact that calcium sulfate chains parallel to [010] in anhydrite structure are very rough.

The strong growth anisotropy affecting anhydrite (100) surface is also reflected by the movement of monolayers along [001] and [00$\bar{1}$]. As explained above, these directions alternate as fast- and slow-moving directions in successive monolayers. Shindo et al.[21−25] pointed out that the calcium sulfate chains which extend along ⟨001⟩ are strongly polar (Figure 7a,b), with this polarity alternating in successive monolayers. As can be observed in Figure 7c, S═O bonds of all the sulfate groups alternately tilt to [001] and [00$\bar{1}$] in successive half unit cell high monolayers. The direct consequence of this feature is that, in anhydrite structure, half unit cell monolayers contain two different types of ⟨010⟩ steps. In a given monolayer the geometry of the steps that advance along [001] is nonequivalent to the geometry of the steps that advance along [00$\bar{1}$] but equivalent to the steps that advance along [00$\bar{1}$] in the monolayers immediately above and underneath. The nonequivalence of parallel [010] steps in a given monolayer is due to the absence of symmetry operators that relate the two types of steps within that monolayer. However, the existence of a 2_1 axis along [100] relates [010] steps advancing in one direction (either [001] or [00$\bar{1}$]) in one monolayer to [010] steps advancing to the opposite direction in the next monolayers. Nonequivalence of parallel steps has been referred to as a main factor determining highly anisotropic growth in a number of crystalline phases. The most widely studied example is calcite (and other calcite-type carbonates), in whose structure the existence of two types of nonequivalent parallel ⟨$\bar{4}$41⟩ steps, one type containing open kink sites and the other containing constrained, less accessible kink sites, determines significant differences in spreading rates. These differences have been widely discussed for the cases of calcite[39−43] and magnesite.[44,45]

Observed differences in the monolayer spread speed along [001] and [00$\bar{1}$] on anhydrite (100) can thus be interpreted as resulting from differences in kink site geometry in the two types of parallel ⟨010⟩ steps (see Figure 7b), which in turn determine different accessibility of the solution to the kink sites and different unit growth incorporation kinetics.

Fast-moving ⟨010⟩ steps are very unstable and rapidly disappear into dendritelike growth fronts. The rough steps that bound dendrites in these growth fronts can be described as vicinal to [001] and [011] steps, that is, they result from the combination of small sectors of straight and more stable steps parallel to [001] and [011]. Changes in the relative contribution of these two types of straight steps to the construction of the rough steps, that is, changes in the step vicinality of the rough steps, lead to changes in the overall step orientation. Both [001] and [011] directions coincide with the orientation of strongly bonded calcium sulfate chains in anhydrite structure[21,22]. The chains that extend along [001] are very straight, as explained above, while the chains that extend along [011] are rougher and contain a higher kink density. In anhydrite (100) surface the steps approach angles close to 60°, which roughly corresponds to that between [012] and [0$\bar{1}$2] directions, at high supersaturations and temperatures, while step angle is ~10°, close to that defined by [01 11] and [0 $\bar{1}$ 11], at lower supersaturations and temperatures (Figure 8a). The actual orientation of the jagged steps bounding the dendrites is controlled by their degree of vicinality (Figure 8b). A change in vicinality is followed by a change in the angle defined by these steps. Our observations

show that step vicinality is less important as supersaturation and/or temperature are higher. Jordan et al.[44] observed changed vicinality of steps in magnesite (104) surface dissolving in contact with acidic solutions and interpreted it as resulting from changes in the proportion of different types of kinks in the steps. This interpretation was supported by the results of a two-dimensional kinetic Monte Carlo (KMC) simulation performed for calcite,[46] which demonstrated that anisotropy in detachment rates of different types of kinks causes step vicinality. According to the kink dynamics approach, our observations seem to indicate that the anisotropy in the attachment rates in different types of kinks is maximum at low supersaturations and temperatures, progressively decreasing as supersaturation and temperature increase.

Evolution of the two-dimensional island shape, characterized by reduction of two-dimensional island elongation and increase of the angle between steps bounding the islands, is also consistent with less anisotropic growth as supersaturation and/or temperature increases.

Spiral Growth Mechanism. Spiral growth is also clear evidence for the highly anisotropic behavior of anhydrite (100) surface. Screw dislocations supply monolayers that alternately move fast along [001] and $[00\bar{1}]$ directions. Most noteworthy is the formation of bilayer steps when a fast-moving monolayer step catches up and combines with a slow-moving monolayer step. Such bilayer steps advance slowly, are rough, and can be described as vicinal to [001] and [011], in a similar way as steps bounding dendrites in fast-moving growth fronts. The formation of bilayer steps around the emergence point of screw dislocations in anhydrite (100) surface has been previously observed during dissolution of this face in contact with undersaturated solutions containing NH_4Cl_2.[25] Formation of bilayer steps is a well referred phenomenon commonly observed during the dissolution and growth of crystal surfaces that contain asymmetric directions and are perpendicular to a 2_1 screw axis. This is the case, for example, of (001) surface in barite-type crystals, namely, barite and celestite.[25,47] During both the spread and the retreat of steps in barite or celestite (001) surface, fast-moving steps catch up to slow-moving steps, both of them half unit cell in height, defining a one-unit cell layer that will move at the same speed as the slow-moving step. The formation of bilayer slow-moving steps in screw dislocations in barite (001) surface determines that spirals increasingly become tightly wound around the core with very little lateral growth, which has led to the conclusion that spiral growth mechanism is kinetically irrelevant in the case of barite-type crystals due to structure-induced self-inhibition.[47] Such a self-inhibition of spiral growth would be expected whenever a crystal surface contained highly anisotropic directions and was perpendicular to a 2_1 screw axis that determined its growth to occur by half unit cell monolayers, which is the case of anhydrite (100) surface. However, no tightening of spirals around the core of screw dislocations was observed in our experiments. The spread rate of the monolayers originating in screw dislocations strongly changed during their spread, depending on the orientation of the bounding steps. Spread rate is maximum for monolayer steps and becomes minimum when bilayer steps form. The overall efficiency of spiral growth in anhydrite (100) surface is controlled by the arrival of fast-moving half unit cell growth fronts that connected with the lower slow-moving monolayer in the bilayer steps, providing a surface for the upper monolayer to resume its fast movement. In our experiments, growth fronts may have originated either from cleavage steps or from the interference of spirals with other approaching steps, which may provide a means for spiral growth to remain an active growth mechanism in highly anisotropic surfaces that grow through half unit cell monolayers.

Implications for Crystallization in the $CaSO_4-H_2O$ System. The growth mechanism of two-dimensional nucleation does not seem to occur at $T < 80$ °C and $\beta_{anh} < 2$ and has a limited contribution to the growth of anhydrite (100) surface at higher temperatures and supersaturations. Therefore, under these conditions, screw dislocations are a relevant source of new steps, allowing growth on anhydrite (100) surface to proceed. However, the efficiency of the spiral growth mechanism on this surface is highly dependent on the interaction between monolayers originating from different dislocations. If the screw dislocation density on anhydrite (100) is low, the efficiency of spiral growth mechanism will also be low due to the reduced probability of interaction between monolayers originating in different dislocations to occur. General conclusions cannot be drawn from growth characteristics of a single surface, even if this surface is, together with (010), the most important one in the habit of anhydrite natural crystals. However, the reported growth behavior of anhydrite (100) at the nanoscale can help to explain why most attempts to obtain anhydrite crystals in the laboratory in the temperature range 60−100 °C have been unsuccessful.[16] HAFM experiments showed that, in contact with supersaturated solutions, gypsum (010) surface continued to grow at temperatures well above 60 °C, with quickly increasing growth rates as the temperature increased up to 120 °C.[48] Above this temperature, gypsum surface rapidly dissolved. Van Driessche et al.[4] in situ measured spread speeds on gypsum (010) surface higher than 300 nm/s when this phase grows at 75.7 °C from an aqueous solution with $\beta_{anh} = 1.4$. Under similar temperature and supersaturation conditions, measured spread speeds on anhydrite (100) surface are remarkably slower, around 2 nm/s. If we assume that subcritical nuclei of gypsum and anhydrite can coexist in an aqueous solution that is supersaturated with respect to both phases, the much slower kinetics of anhydrite growth together with the peculiar characteristics of spiral growth and the high supersaturation required for the formation of two-dimensional nuclei on anhydrite (100) surface can explain the metastable development of gypsum crystals under temperatures corresponding to the stability field of anhydrite.

ASSOCIATED CONTENT

Supporting Information. One table, showing solution composition summary (temperature, concentration of stock solution added, calculated activities of reactants, and supersaturation). This material is available free of charge via the Internet at http://pubs.acs.org.

AUTHOR INFORMATION

Corresponding Author

*Telephone +34-91-394-4876; e-mail lfdiaz@geo.ucm.es.

ACKNOWLEDGMENT

We thank Guntram Jordan for generously providing access to the hydrothermal atomic force microscope and training J.M. in using it. This work has been funded by Projects CGL2007- 65523-C02-01 and CGL2010-20134-C02-01 (MICINN-Spain). J.M. is grateful to the Spanish Ministry of Science and Innovation

for a FPI fellowship. The comments of two reviewers, which helped to improve the paper, are also acknowledged.

REFERENCES

(1) Anthony, J. W.; Bideaux, R. A.; Bladh, K. W.; Nichols, M. C. Handbook of Mineralogy, Vol. V. Borates, Carbonates, Sulfates; Mineral Data Publishing: Tucson, AZ, 2003.

(2) Tucker, M. E. Sedimentary Petrology: An introduction to the origin of sedimentary rocks, 3rd ed.; Wiley□Blackwell: Oxford, U.K., 2001.

(3) García-Ruiz, J. M.; Villasuso, R.; Ayora, C.; Canals, A.; Otalora, F. Geology 2007, 35, 327–330.

(4) Van Driessche, A. E. S.; García-Ruiz, J. M.; Delgado-L´opez, J. M.; Sazaki, G. Cryst. Growth Des. 2010, 10, 3909–3916.

(5) Kuhn, T.; Herzig, P. M.; Hannington, M. D.; Garbe-Sch€onberg, D.; Stoffers, P. Chem. Geol. 2003, 202, 5 –21.

(6) Kuwahara, Y. Geochim. Cosmochim. Acta 2011, 75, 4 1 –51.
(7) Kawada, Y.; Yoshida, S. J. Geophys. Res. 2010, 115, B11106.
(8) Schmidt, K.; Garbe-Sch€onberg, D.; Bau, M.; Koschinsky, A. Geochim. Cosmochim. Acta 2010, 74, 4058–4077.

(9) Kennedy, B. A. Surface Mining. Society for Mining, Metallurgy and Exploration, Inc.: Baltimore, MD, 1991.

(10) Amjad, Z. J. Colloid Interface Sci. 1998, 123, 523–536.

(11) Fan, C.; Kan, A. T.; Fu, G.; Tomson, M. B.; Shen, D. SPE J. 2010, 15 (4), 977–988.

(12) Gill, J. S.; Nancollas, G. H. J. Cryst. Growth 1980, 48, 3 4 –40.(13) Nancollas, G. H.; Reddy, M. M.; Tsai, F. J. Cryst. Growth 1973, 20, 125–134.

(14) Bosbach, D.; Rammensee, W. Geochim. Cosmochim. Acta 1994, 58, 843–849.

(15) Bosbach, D.; Jordan, G.; Rammensee, W. Eur. J. Mineral 1995, 7, 267–276.

(16) Freyer, D.; Voigt, W. Monatsh. Chem. 2003, 134, 693–719.(17) Jordan, G.; Astilleros, J. M. Am. Mineral. 2006, 91, 619–627.(18) Fan, C.; Teng, H. H. Chem. Geol. 2007, 245, 242–253.
(19) Posnjak, E. Am. J. Sci. 1938, 235-A, 247–272.
(20) Hardie, L. A. Am. Mineral. 1967, 52, 171–200.
(21) Shindo, H.; Nozoye, H. J. Chem. Soc., Faraday Trans. 1992, 88, 711–714.

(22) Shindo, H.; Kaise, M.; Kondoh, H.; Nishihara, C.; Nozoye, H. Appl. Surf. Sci. 1992, 60/6, 491–497.

(23) Shindo, H.; Seo, A.; Itasaka, M.; Odaki, T.; Tanaka, K. J. Vac. Sci. Technol. 1996, B14 (2), 1365–1368.

(24) Shindo, H.; Shitagami, K.; Kondo, S.; Seo, A. J. Cryst. Growth 1999, 198/199, 253–257.

(25) Shindo, H.; Shitagami, K.; Sugai, T.; Kondo, S. Phys. Chem. Chem. Phys. 1999, 1, 1597–1600.

(26) Shindo, H.; Seo, A.; Watabe, T. Phys. Chem. Chem. Phys. 2001, 2, 230–234.

(27) Shindo, H.; Igarashi, T.; Karino, W.; Seo, A.; Yamanobe-Hada, M.; Haga, M. J. Cryst. Growth 2010, 312, 573–579.

(28) Pina, C. M.; Fern´andez-Díaz, L. Geochim. Cosmochim. Acta 2007, 71, 793–793.

(29) Pina, C. M. Geochim. Cosmochim. Acta 2009, 73, 7034–7044.

(30) Hawthorne, F. C.; Ferguson, R. B. Can. Mineral 1975, 13, 289–292.

(31) Hawthorne, F. C.; Krivovichev, S. V.; Burns, P. C. Rev. Mineral. Geochem. 2000, 40, 1 –112.

(32) Redfern, S. E.; Parker, S. C. J. Chem. Soc., Faraday Trans. 1998, 94, 1947–1952.

(33) Hartman, P.; Perdok, W. G. Acta Crystallogr. 1955, 8, 4 9 –52.(34) Hartman, P.; Perdok, W. G. Acta Crystallogr. 1955, 8, 521–524.(35) Higgins, S. R.; Jordan, G.; Eggleston, C. M. Langmuir 1998, 14, 4967–4971.

(36) Higgins, S. R.; Eggleston, C. M.; Knauss, K. G.; Boro, C. O. Rev. Sci. Instrum. 1998, 69, 2994–2998.

(37) Parkhurst, D. L.; Appelo, C .A . J. In User's guide to PHREEQC (Version 2): A computer program for speciation, batch-reaction, one-dimensional transport and inverse geochemical calculations. U.S. Geological Survey Water Resources Investigations Report, Washington, DC, 2003.

(38) CrystalMaker Software, P. O. Box 183, Bicester, Oxfordshire OX6 7BS, U.K. http://www.crystalmaker.com.

(39) Staudt, W. J.; Reeder, R. J.; Schoonen, M. A. A. Geochim. Cosmochim. Acta 1994, 58, 2087–2098.

(40) Paquette, J.; Reeder, R. J. Geochim. Cosmochim. Acta 1995, 59, 735–749.

(41) Reeder, R. J.; Rakovan, J.; Jamtveit, B.; Meakin, P., Eds. Growth, Dissolution and Pattern Formation in Geosystems: Kluwer Academic Publishers: Dordrecht, The Netherlands, 1999.

(42) Leeuw, N. H.; Parker, S. C. Phys. Rev. B 1999, 60, 13792–13799.

(43) Teng, H.; Dove, P. M.; De Yoreo, J. J. Geochim. Cosmochim. Acta 2001, 64, 2255–2266.

(44) Jordan, G.; Higgins, S. R.; Eggleston, C. M.; Knauss, K. G.; Schmahl, W. W. Geochim. Cosmochim. Acta 2001, 65, 4257–4266.

(45) Jordan, G.; Pokrovsky, O. S.; Guichet, X.; Schmahl, W. W. Chem. Geol. 2007, 242, 484–496.

(46) McCoy, J. M.; LaFemina, J. P. Surf. Sci. 1997, 373, 288–299.

(47) Pina, C. M.; Becker, U.; Risthaus, P.; Bosbach, D.; Putnis, A. Nature 1998, 395, 483–486.

(48) Jordan, G.; Astilleros, J. M. Am. Mineral. 2006, 91, 619–627.